JBC ARTICLE

⌘ Author's Choice

Molecular basis of cullin-3 (Cul3) ubiquitin ligase subversion by vaccinia virus protein A55

Received for publication, November 4, 2018, and in revised form, February 26, 2019 Published, Papers in Press, February 28, 2019, DOI 10.1074/jbc.RA118.006561

Chen Gao[‡], Mitchell A. Pallett[‡], Tristan I. Croll[§], Geoffrey L. Smith[‡], and Stephen C. Graham[‡1]

From the [‡]Department of Pathology, University of Cambridge, Tennis Court Road, Cambridge CB2 1QP and the [§]Cambridge Institute for Medical Research, University of Cambridge, Wellcome Trust/MRC Building, Cambridge CB2 0XY, United Kingdom

Edited by Wolfgang Peti

BTB–Kelch proteins are substrate-specific adaptors for cullin-3 (Cul3) RING-box–based E3 ubiquitin ligases, mediating protein ubiquitylation for subsequent proteasomal degradation. Vaccinia virus encodes three BTB–Kelch proteins: A55, C2, and F3. Viruses lacking A55 or C2 have altered cytopathic effects in cultured cells and altered pathology *in vivo*. Previous studies have shown that the ectromelia virus orthologue of A55 interacts with Cul3 in cells. We report that the N-terminal BTB-BACK (BB) domain of A55 binds directly to the Cul3 N-terminal domain (Cul3–NTD), forming a 2:2 complex in solution. We solved the structure of an A55BB/Cul3–NTD complex from anisotropic crystals diffracting to 2.3/3.7 Å resolution in the best/worst direction, revealing that the overall interaction and binding interface closely resemble the structures of cellular BTB/Cul3–NTD complexes, despite low sequence identity between A55 and cellular BTB domains. Surprisingly, despite this structural similarity, the affinity of Cul3–NTD for A55BB was stronger than for cellular BTB proteins. Glutamate substitution of the A55 residue Ile-48, adjacent to the canonical *ϕX*(D/E) Cul3-binding motif, reduced affinity of A55BB for Cul3–NTD by at least 2 orders of magnitude. Moreover, Ile-48 and the *ϕX*(D/E) motif are conserved in A55 orthologues from other poxviruses, but not in the vaccinia virus proteins C2 or F3. The high-affinity interaction between A55BB and Cul3–NTD suggests that, in addition to directing the Cul3–RING E3 ligase complex to degrade cellular/viral target proteins that are normally unaffected, A55 may also sequester Cul3 from cellular adaptor proteins, thereby protecting substrates of these cellular adaptors from ubiquitylation and degradation.

Vaccinia virus (VACV)[2] is a dsDNA virus in the *Orthopoxvirus* genus of the Poxviridae. Historically, VACV was used as the vaccine to eradicate smallpox (1). Its genome contains ~200 genes, about half of which are involved in the modulation of host immune response to viral infection, and the virus has been used as a model system to study innate immunity (2). The mechanisms by which several VACV proteins act to inhibit innate immune sensing and effector function, especially those involved in the inhibition of NF-κB signaling, have been well characterized (2, 3). Nevertheless, many VACV immunomodulatory proteins are still poorly understood, and one such protein is A55.

A55 is an intracellular protein encoded by the *A55R* gene of VACV (4). It belongs to the BTB (Bric-a-brac, Tramtrack, and Broad complex)-Kelch protein family, which are substrate adaptor proteins specific for the cullin-3 (Cul3)-RING (Really Interesting New Gene)–based E3 ubiquitin ligase (C3RL) complex (5). The N-terminal region of these proteins contains a BTB domain that mediates dimerization and binding to Cul3, a three-box helical bundle region, and a BACK (for BTB and C-terminal Kelch) domain that is likely responsible for correctly orienting the C terminus (5–13). The C-terminal region comprises 4–6 Kelch repeats arranged into a single β-propeller that captures the substrates for the C3RL complex; alternatively, these Kelch domains may also interact with actin filaments to regulate cytoskeleton organization (5, 9–11, 14–19). In cells, there are many BTB domain–containing proteins conjugated with different substrate recognition domains, and their interactions with various substrates and C3RL complexes are implicated in several cellular processes, including protein degradation, transcriptional regulation (KEAP1), the gating of voltage-gated potassium channels (KCTDs), and cytoskeleton modulation (KLHLs) (19–25). Apart from mimiviruses, poxviruses are the only family of viruses that make BTB domain–containing proteins (26–30).

This work was supported by Wellcome Trust Principal Research Fellowship 090315 (to G. L. S.) and Sir Henry Dale Fellowship 098406/Z/12/B, jointly funded by the Wellcome Trust and the Royal Society (to S. C. G.). The authors declare that they have no conflicts of interest with the contents of this article.

⌘ *Author's Choice*—Final version open access under the terms of the Creative Commons CC-BY license.

This article contains Figs. S1–S7 and supporting Refs. 1–5.

The atomic coordinates and structure factors (code 6I2M) have been deposited in the Protein Data Bank (http://wwpdb.org/).

Raw diffraction images have been deposited in the University of Cambridge Apollo repository (https://doi.org/10.17863/CAM.33381). (Please note that the JBC is not responsible for the long-term archiving and maintenance of this site or any other third party hosted site.)

[1] To whom correspondence should be addressed: Dept. of Pathology, University of Cambridge, Tennis Court Rd., Cambridge CB2 1QP, United Kingdom. Tel.: 44-1223336920; E-mail: scg34@cam.ac.uk.

[2] The abbreviations used are: VACV, vaccinia virus; BACK, BTB and C-terminal Kelch; BTB, Bric-a-brac, Tramtrack and Broad-complex; BB, BTB–three-box–BACK domain; DSF, differential scanning fluorimetry; ECTV, ectromelia virus; EV, empty vectors; IEF, isoelectric focusing; IPTG, isopropyl β-D-1-thiogalactopyranoside; ITC, isothermal titration calorimetry; KCTD, potassium channel tetramerization domain protein; KLHL, kelch-like protein; MALS, multiangle light-scattering; NTD, N-terminal domain; NTE, N-terminal extension; POZ, poxvirus and zinc finger; RING, really interesting new gene; SEC, size-exclusion chromatography; SPOP, speckle-type POZ (poxvirus and zinc finger) protein; TAP, tandem affinity purification; TEV, tobacco etch virus; PDB, Protein Data Bank; DMEM, Dulbecco's modified Eagle's medium; aa, amino acid; WR, Western Reserve; IP, immunoprecipitation.

© 2019 Gao et al. Published by The American Society for Biochemistry and Molecular Biology, Inc.

Deletion of A55 from VACV does not diminish virus replication in cultured cells (4). However, cells infected with VACV lacking A55 (vΔA55) demonstrated altered cytopathic effects, including the loss of Ca^{2+}-independent cell adhesion and cellular projections, suggesting that A55 plays a role in the modulation of the cytoskeleton (4). The use of an intradermal murine model of infection demonstrated that infection with vΔA55 caused increased lesion size compared with WT virus, suggesting that A55 plays a role in altering the host immune response *in vivo* (4).

VACV encodes three BTB–Kelch proteins, namely A55, C2, and F3. Despite having similar domain organizations, A55 shares limited sequence identity with C2 and F3 (22 and 25%, respectively). Like A55, C2 and F3 are dispensable for VACV replication in cultured cells (31, 32). Infection of cells with vΔA55 or with VACV lacking C2 (vΔC2) produced a similar loss of Ca^{2+}-independent cell adhesion, suggesting that A55 and C2 affect similar cellular pathways (4, 31). However, intradermal infection *in vivo* with vΔC2 resulted in similar-sized lesions to WT infection, but these lesions persisted longer, distinct from the phenotype observed for vΔA55 (4, 31). Infection with VACV lacking F3 (vΔF3) produced no distinct phenotype in cultured cells, but intradermal infection yielded smaller lesions compared with WT virus (32). These results suggest that VACV BTB–Kelch proteins are functionally divergent despite having a conserved domain organization.

C3RLs are a family of multimodular cullin-RING–based E3 ubiquitin ligases that recruit substrates specifically via BTB domain–containing adaptor proteins (5, 6). Cul3, the all-helical stalk-like scaffold subunit of C3RLs, interacts directly with BTB domain–containing proteins via its N-terminal domain (6–8, 13, 24, 33). The C-terminal domain of Cul3 interacts with the RING-based E3 ligase protein to recruit the ubiquitin-loaded E2–conjugating enzyme for substrate ubiquitylation and is dispensable for binding to BTB domain proteins (5, 11, 34). Crystal structures of several cellular BTB domain proteins in complex with the Cul3 N-terminal domain (Cul3–NTD) have been reported (6, 7, 13, 24). These structures revealed a unique mode of binding of BTB-containing adaptor proteins to the C3RL family of E3 ubiquitin ligases. Interaction with Cul3 is mainly via the BTB domain, with additional contacts from the three-box region, whereas the BACK domain does not participate in the binding. The N-terminal 22 residues of Cul3 (N-terminal extension (NTE)) are usually disordered and dispensable for binding, and many reported binding studies of BTB domain–containing proteins to Cul3 were carried out with N-terminally truncated Cul3–NTD ($Cul3_{20-381}$ for KLHL3, SPOP, and KCTD5, $Cul3_{23-388}$ for KLHL11, and $Cul3_{26-381}$ for KEAP1) (6, 7, 13, 24). However, the Cul3–NTE does provide extra hydrophobic contacts with the three-box region upon binding to KLHL11 and KCTD5, resulting in significant increases in affinity (6, 25).

Ubiquitin ligases act together with the proteasome to regulate the turnover of a large number of cellular proteins. Many viruses exploit the ubiquitylation–proteasomal degradation pathways to ensure successful infection and spread (35–41). To achieve this, viruses have evolved proteins that interact with ubiquitin ligase complex components to subvert the degradation pathways (35, 37, 39, 42, 43).

The ectromelia virus (ECTV) orthologue of A55, EVM150, shares 93% sequence identity to A55. EVM150 has been reported to interact with Cul3 via its BTB domain and co-localizes with the C3RL and conjugated ubiquitin in cells (43). In addition, the BTB domain of EVM150 was reported to inhibit NF-κB signaling, although Cul3 appeared dispensable for this activity (42).

In this study, we showed that A55 binds directly to Cul3 and solved the crystal structure of a complex between Cul3–NTD and the BTB-BACK (BB) domain of A55. Although the overall conformation of the complex is similar to reported cellular BTB/Cul3–NTD structures, Cul3–NTD binds A55BB more tightly than it does cellular BTB proteins. This strong A55/Cul3 interaction may allow VACV to redirect the E3 ubiquitin ligase complex to degrade novel target proteins and/or to subvert cellular BTB/Cul3–NTD interactions to rescue proteins from degradation.

Results

A55 binds to Cul3 of the E3 ubiquitin ligase complex via its N-terminal BB domain

Poxvirus BTB–Kelch protein EVM150 has been shown to co-precipitate with Cul3 and modulate innate immune responses upon infection (42, 43). A55 is also predicted to have a BTB–Kelch domain architecture and shares 93% aa identity to EVM150. To test whether A55 interacts with Cul3, co-immunoprecipitation experiments were performed using inducible HEK293T–REx cell lines expressing A55 with a FLAG-containing tandem affinity purification (TAP) tag at its N terminus (TAP–A55) or B14, an NF-κB inhibitor from VACV (44), with a C-terminal TAP tag (B14–TAP). Endogenous Cul3 co-immunoprecipitated with TAP–A55, but not B14–TAP, when overexpressed in HEK293T–REx cells (Fig. 1*A*). This suggests that Cul3 specifically co-immunoprecipitates with A55 and not with other VACV immune modulatory proteins. Furthermore, TAP–A55 co-immunoprecipitated with N-terminally Myc-tagged Cul3 (myc-Cul3) but not with myc-Cul5, suggesting that A55 interacts specifically with Cul3 and not with other cullin family proteins (Fig. 1*B*). To dissect the region of A55 that binds to Cul3, the BB and Kelch domains of A55 were tagged at the N terminus with TAP and were immunoprecipitated after overexpression in HEK293T–REx cells. Endogenous Cul3 co-immunoprecipitated with the N-terminal BB domain but not with the C-terminal Kelch domain (Fig. 1*C*). These results suggest that, like the ECTV BTB–Kelch protein EVM150, A55 interacts with Cul3 and that this interaction is mediated solely by the N-terminal BB domain.

A55 is an obligate dimer in solution and forms a 2:2 complex with Cul3

Previous biochemical and structural analysis has shown that Cul3 binds cellular BTB–Kelch proteins via its N terminus (residues 1–388), while its C terminus (389–767) is not required for binding (6–8, 13). To test whether A55 forms a direct complex with Cul3 in solution, the A55 BB domain (A55BB, residues 1–250) and the Cul3 N-terminal domain (Cul3NΔ22, residues 23–388) were expressed in *Escherichia coli* and purified according to protocols described under "Experimental procedures." Size-exclusion chromatography coupled to

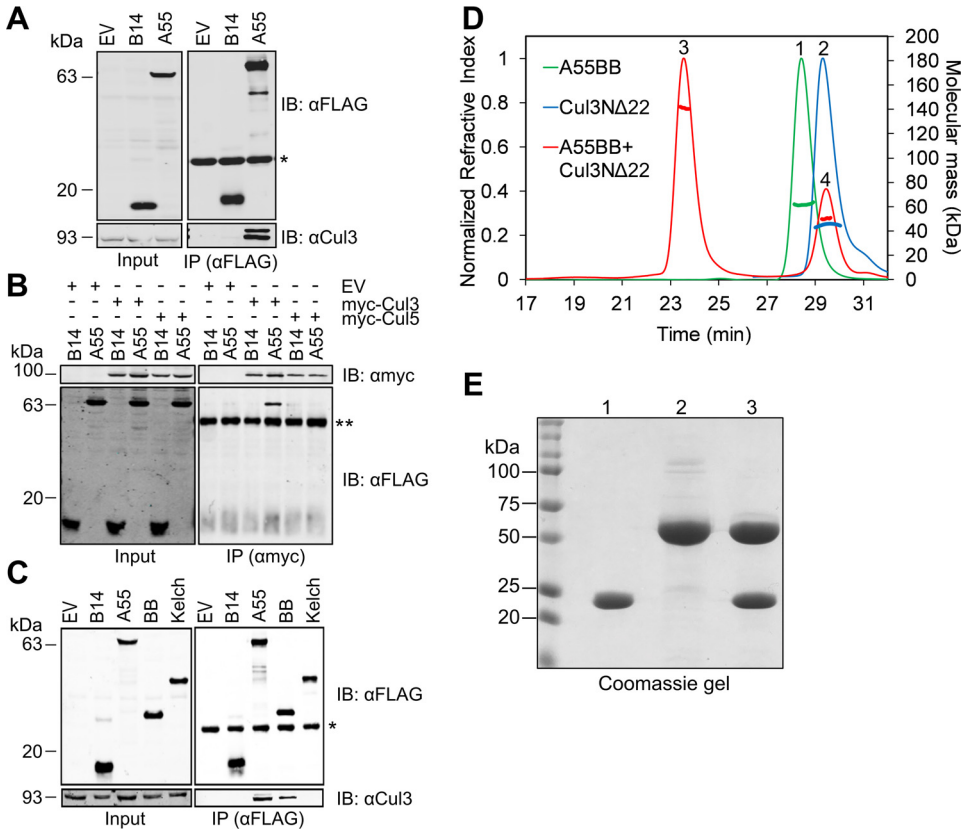

Figure 1. A55 directly binds to cullin-3 via its N-terminal BB domain. *A–C,* representative immunoblots following immunoprecipitation (*IP*) of cleared lysates from HEK293T–REx cell lines (*A*) expressing empty vector (*EV*), B14–TAP (*B14*), or TAP–A55 (*A55*), the TAP tag comprising STREP and FLAG epitopes; (*B*) expressing B14–TAP or TAP–A55 and transfected with plasmids encoding myc-Cul3 or myc-Cul5; (*C*) expressing EV, B14–TAP, TAP–A55, TAP–A55BB, or TAP–A55 Kelch. Cells were lysed in Nonidet P-40 (*A* and *C*) or RIPA buffer (*B*). Immunoprecipitates were subjected to SDS-PAGE and immunoblotting. *A* and *C,* FLAG IP and immunoblotting for co-IP of endogenous Cul3. *B,* Myc IP and immunoblotting for co-IP of TAP-tagged B14 or A55. *Input,* cleared lysate. Data shown are representative of at least three independent experiments. Signals arising from the light chain (*) or heavy chain (**) of the antibody used for IP are marked. *D,* SEC-MALS analyses showing the SEC elution profiles (*thin lines*) and molecular mass distribution (*thick lines*) across the elution peaks for A55BB (*peak 1, green,* theoretical molecular mass 30 kDa and observed molecular mass 60 kDa), Cul3NΔ22 (*peak 2, blue,* theoretical molecular mass 46 kDa and observed molecular mass 45 kDa), and A55BB and Cul3NΔ22 together (*peak 3, red,* theoretical molecular mass 76 kDa and observed molecular mass 141 kDa) when eluting from a Superdex 200 10/300 GL column. *Peak 4* is assumed to be excess Cul3NΔ22. *E,* Coomassie-stained SDS-PAGE analysis of *peaks 1–3* from *D*.

multiangle light-scattering (SEC-MALS) studies together with SDS-PAGE analysis showed that A55BB exists as a homodimer in solution (expected molecular mass 60 kDa) (Fig. 1*D*). This is consistent with observations for other cellular BTB proteins (6–8). Cul3NΔ22 is monomeric (expected molecular mass 46 kDa). However, when A55BB and Cul3NΔ22 were mixed at ~1:1 molar ratio, a complex was formed with an apparent molecular mass of 141 kDa, consistent with a 2:2 complex of A55BB/Cul3NΔ22 (expected molecular mass 152 kDa) (Fig. 1, *D* and *E*). Overall, the results show that A55 is dimeric in solution and binds directly to Cul3 to form a heterotetramer.

A55 binds to Cul3 with low- to sub-nanomolar affinity

Isothermal titration calorimetry (ITC) experiments were carried out to determine the binding affinity between A55BB and Cul3. Two different truncations of Cul3 containing the N-terminal domain were used: Cul3N (residues 1–388) and Cul3NΔ22 (residues 23–388) to compare the binding affinities between A55 and Cul3 with or without the Cul3–NTE. A55BB formed equimolar complexes with both Cul3NΔ22 and Cul3N with affinities in the low nanomolar (5.3 ± 2.9 nM) and sub-nanomolar (<1 nM) range, respectively (Fig. 2, *A* and *B*; Table 1). The binding affinity of A55BB for Cul3N could not be determined accurately as rapid depletion of free Cul3N in the cell upon the introduction of A55BB prevented fitting of the resultant titration data to a single-site binding model. Attempts to lower the concentrations of A55BB and Cul3N or to use displacement titration experiments (45) were unsuccessful due to limitations of instrument sensitivity. Previous studies have shown cellular BTB proteins to bind the Cul3 N-terminal domain with much lower affinities than observed for A55BB (6–8, 13). To facilitate a direct comparison, the binding of KLHL3-BB to Cul3N and Cul3NΔ22 was measured by ITC (Fig. 2, *C* and *D*). These experiments confirmed that the affinity of Cul3–NTD for A55BB is ~10-fold tighter than for KLHL3-BB (Fig. 2, *C* and *D*; Table 1). Interestingly, the affinity of A55BB for Cul3NΔ22 was stronger despite the enthalpic contribution to the interaction ($\Delta H = -9.9 \pm 0.8$ kcal/mol) being lower than for the equivalent interaction between KLHL3-BB and Cul3NΔ22 ($\Delta H = -18.9 \pm 2.0$ kcal/mol) (Table 1). This suggests that the tighter interaction arises from a more favorable entropic contribution upon complex formation, such as the burial of exposed hydrophobic regions leading to the release of ordered solvent molecules and/or less conformational restriction of A55 upon complex formation. Taken together, the ITC data presented here show that the VACV A55BB

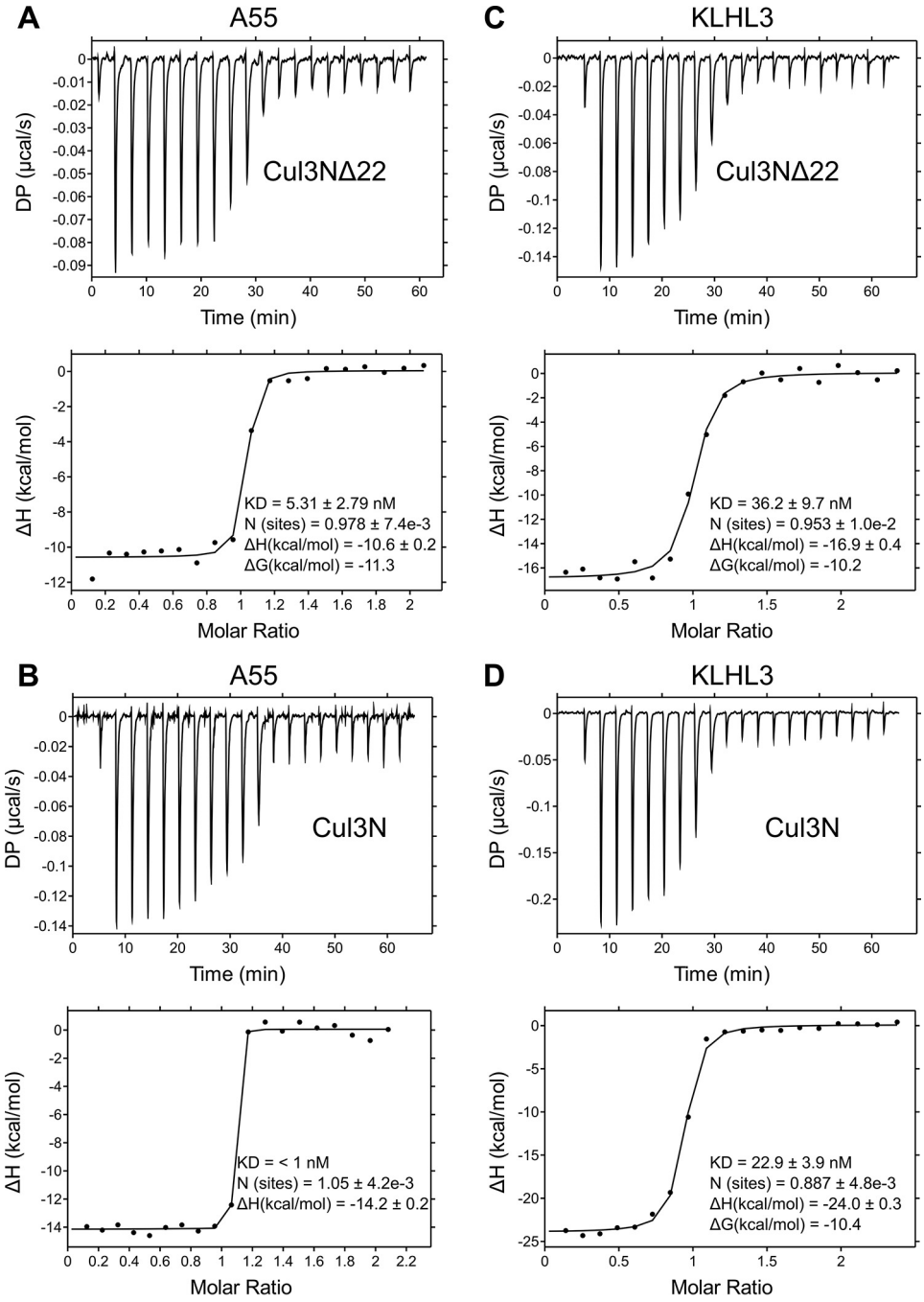

Figure 2. ITC studies show that A55 binds to Cul3 with nanomolar to sub-nanomolar affinity. *A–D,* representative ITC titration curves showing interactions between A55BB and Cul3NΔ22 (*A*) or Cul3N (*B*) and between KLHL3, a human BTB related to A55, and Cul3NΔ22 (*C*) or Cul3N (*D*). The *top figure* in each panel shows the baseline-corrected differential power (*DP*) *versus* time. The *bottom figure* of each panel is the normalized binding curve showing integrated changes in enthalpy (Δ*H*) against molar ratio. The corresponding dissociation constant (K_D), number of binding sites (*N*), enthalpy change (Δ*H*), and change in Gibbs free energy (Δ*G*) for each representative experiment are shown. All experiments were performed at least twice independently.

binds Cul3–NTD more tightly than previously-studied cellular BTB domain–containing proteins (Table 1) and that different thermodynamic properties of the interaction contribute to this enhanced binding.

Determination of the A55BB/Cul3NΔ22 complex structure

To understand the molecular mechanism underlying the observed high-affinity interaction between A55BB and Cul3–NTD, the A55BB/Cul3NΔ22 complex was purified and subjected to extensive crystallization screening for structural characterization. Initial trials did not yield any crystals. To promote crystallization, A55BB was subjected to surface entropy reduction by reductive methylation (46) before being purified in complex with Cul3NΔ22 (Fig. S1). Crystals of methylated (M) A55BB in complex with Cul3NΔ22 grew as thin needles after 2 weeks. By using microseeding and varying the pH and concentration of the precipitants, optimized crystals were grown that diffracted to 2.3 Å in the best direction. Inspection of the dif-

Table 1

Comparison of the dissociation constants (K_D), enthalpic change (ΔH), and entropic change ($T\Delta S$) for BB–Cul3 interaction

Experiments for this study were performed at least twice, and mean ± S.E. is shown.

Protein	Cul3NΔ22			Cul3N		
	K_D	ΔH	$T\Delta S$	K_D	ΔH	$T\Delta S$
	nM	*kcal/mol*	*kcal/mol*	*nM*	*kcal/mol*	*kcal/mol*
A55	5.3 ± 2.9	−9.9 ± 0.8	−1.8 ± 0.8	<1	−17.7 ± .1.1	–[a]
KLHL3	52.8 ± 16.6	−18.9 ± 2.0	9.0 ± 2.3	17.0 ± 5.1	−24.9 ± 0.9	14.2 ± 0.7
$SPOP^{BTB+}$[b]	–	–	–	17[c]	–	–
SPOP	13 ± 2[d]	–	–	–	–	–
KLHL11	650[e]	–	–	20[e]	–	–

[a] Data were not defined because the K_D value could not be accurately measured.
[b] $^{BTB+}$ indicates BTB domain + three-box region.
[c] Value is as reported in Zhuang *et al.* (8).
[d] Value is as reported in Errington *et al.* (13).
[e] Values are as reported in Canning *et al.* (6).

Table 2

A55BB Cul3NΔ22 complex data collection and refinement statistics

Statistics for data from a single crystal before (isotropic) and after anisotropic truncation and scaling using STARANISO (anisotropic) are shown. Statistics for the highest-resolution shell are shown in parentheses.

Data collection		
Beamline	Diamond I04	
Wavelength	0.9795 Å	
Space group	*C* 1 2 1	
Cell dimensions		
a, *b*, *c* (Å)	198.8, 42.5, 148.8	
β (degrees)	128.4	
Scaling procedure	*Isotropic*	*Anisotropic*
Resolution range (Å)	99.2–2.3 (2.36–2.30)	116.6–2.3 (2.51–2.30)
Total reflections	568,838 (41,470)	300,453 (14,478)
Unique reflections	44,144 (3279)	23,509 (1172)
Multiplicity	12.9 (12.6)	12.8 (12.4)
Completeness (%)	100 (99.9)	53.2 (11.6)
Mean(I/σ(I))	8.1 (0.1)	15.3 (2.2)
R_{pim}	0.040 (4.996)	0.025 (0.295)
R_{merge}	0.140 (17.224)	0.087 (1.005)
$CC_{½}$	0.999 (0.302)	1.000 (0.848)
Refinement		
Resolution (Å)		58.3–2.3 (2.30–2.39)
Reflections used in refinement		22,331 (453)
Reflections in test (free) set		1170 (18)
R_{work}		0.266 (0.292)
R_{free}		0.282 (0.246)
Protein residues		539
Number of non-hydrogen atoms		4402
Root mean square deviation		
Bonds length (Å)		0.008
Bond angle (degrees)		0.93
Ramachandran favoured* (%)		93.2
Ramachandran outliers* (%)		0.4
Rotamer outliers* (%)		0.81
Clashscore*		1.6
Average B-factor (Å^2)		73.2

* Data are reported by Molprobity (65).

fraction data suggested severe anisotropy, with significantly worse diffraction along one axis (3.7 Å in direction 0.76 a^* − 0.65 c^*) compared with the other major axes (2.6 Å in the direction b^* and 2.3 Å in the direction 0.92 a^* + 0.39 c^*), so these data were processed with anisotropic scaling and truncation using STARANISO (47) and DIALS (48). The final processed dataset contained 23,509 unique reflections (Table 2), equivalent to the number of reflections expected for a 2.8 Å dataset collected from an isotropically-diffracting crystal with equivalent space group and unit cell dimensions. The anisotropy of diffraction was present in all crystals of the A55BB(M)/Cul3NΔ22 complex for which data were collected (>20 individual crystals).

The structure of A55BB(M)/Cul3NΔ22 crystal was solved by molecular replacement using B-cell lymphoma 6 BTB domain (PDB code 1R29) (49) and $Cul3_{20-381}$ from the SPOP/Cul3 complex structure (PDB code 4EOZ) (13) as the search models. Although most of the Cul3NΔ22 molecule could be modeled with ease, the initial map for A55BB was less well-defined with relatively weak density for the three-box and BACK regions. Anisotropic scaling of the diffraction data and the use of interactive molecular dynamics in ISOLDE (50) improved the model quality and fit to density significantly. The final model was refined using BUSTER (51) and has residuals R_{work}/R_{free} of 0.266/0.282 with good overall geometry. Data collection and refinement statistics are summarized in Table 2. No crystals of A55BB(M) either alone or in complex with Cul3N could be obtained despite extensive crystallization trials.

Structurally A55BB resembles cellular BTB–Kelch proteins with conserved Cul3-binding and dimerization interfaces

The structure of the A55BB(M)/Cul3NΔ22 complex contains one copy of each molecule in the crystallographic asymmetric unit (Fig. 3*A*). Consistent with the SEC-MALS analysis, a heterotetramer of A55BB(M)/Cul3NΔ22 can be observed by applying crystallographic 2-fold symmetry. A55BB dimerization is mediated by the BTB domain, where the N-terminal helix (α1) forms a domain-swapped interaction with the symmetry-related molecule (Fig. 3*B*). The Cul3NΔ22 molecule is all-helical and closely resembles previously solved Cul3 N-terminal domain structures, with root-mean-squared displacement of 0.8 and 0.7 Å across 336 and 339 C^α atoms when aligned to the Cul3 structures in the KLHL3/Cul3NΔ19 (7) and KLHL11/Cul3NΔ22 (6) complexes, respectively (Fig. 3*C*). A55BB consists of a globular BTB domain (residues 1–118; helices α1–α6 and strands β2–β4) followed by a helix–turn–helix three-box region (residues 119–149; helices α7–α8) and an all-helical BACK domain (residues 150–196, helices α9–α12) (Fig. 3*A*). A55BB closely resembles the equivalent regions of KLHL3 and KLHL11 (root-mean-squared displacements of 2.2 and 2.5 Å across 167 and 181 C^α atoms, respectively), despite the low sequence conservation between A55 and these cellular proteins (Fig. S2 and Fig. 4), and the formation of dimers via an N-terminal helix domain swap is a conserved feature of all three proteins (Fig. 3*D*).

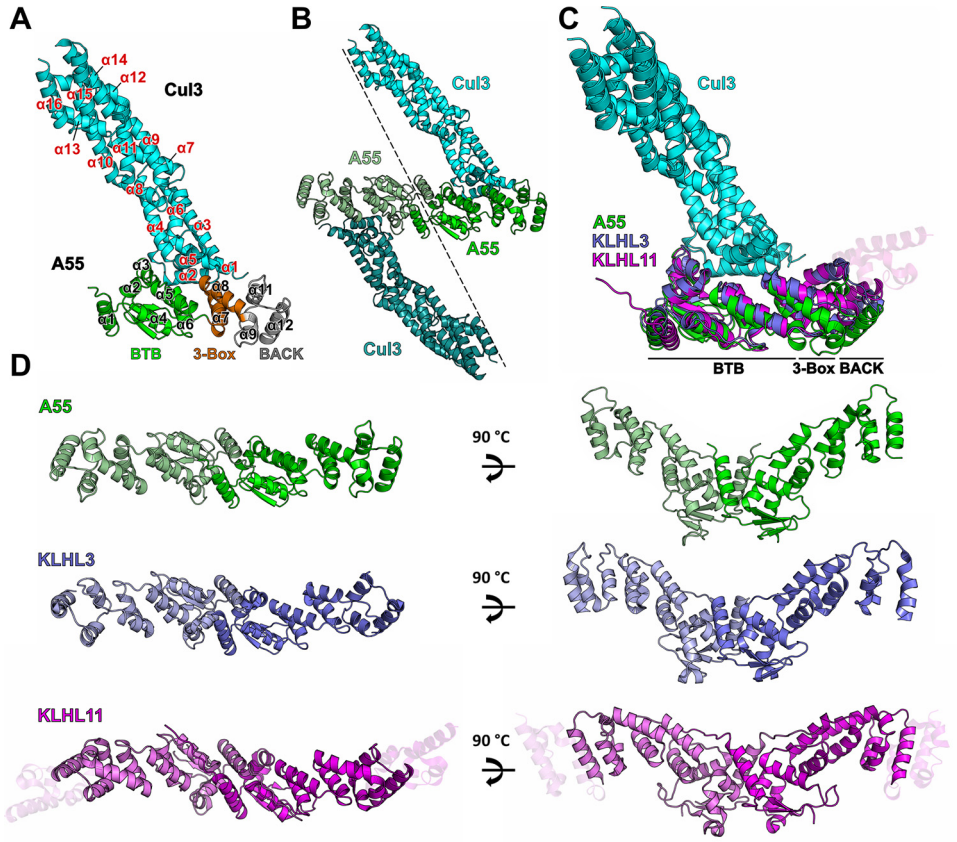

Figure 3. A55 and cellular BB domains share conserved modes of dimerization and Cul3 binding. *A,* structure of the A55/Cul3NΔ22 heterodimer in the asymmetric unit as *ribbon diagram*. Cul3 is in *cyan* and the three domains of A55 (BTB, three-box and BACK) are in *green, orange,* and *gray*, respectively. Helices α1–α12 from A55 are labeled in *black* with the exception of α10, which is hidden behind α9 in the picture. Helices α1–α16 from Cul3 are labeled in *red*. *B,* A55/Cul3 dimer formed by applying crystallographic 2-fold symmetry. *C,* overlay of three BB/Cul3 complex structures (KLHL3/Cul3, PDB code 4HXI (7); KLHL11/Cul3, PDB code 4APF (6); and A55/Cul3). The structures are aligned to the Cul3 part of the A55/Cul3 complex only. A55, KLHL3, KLHL11, and Cul3 are in *green, purple, magenta,* and *cyan*, respectively, and the three sub-domains are marked. Additional helices at the C terminus of the KLHL11 BACK domain are shown as semi-transparent helices. *D,* comparison of the dimers formed by A55, KLHL3, and KLHL11 BB domains, colored as in *C*.

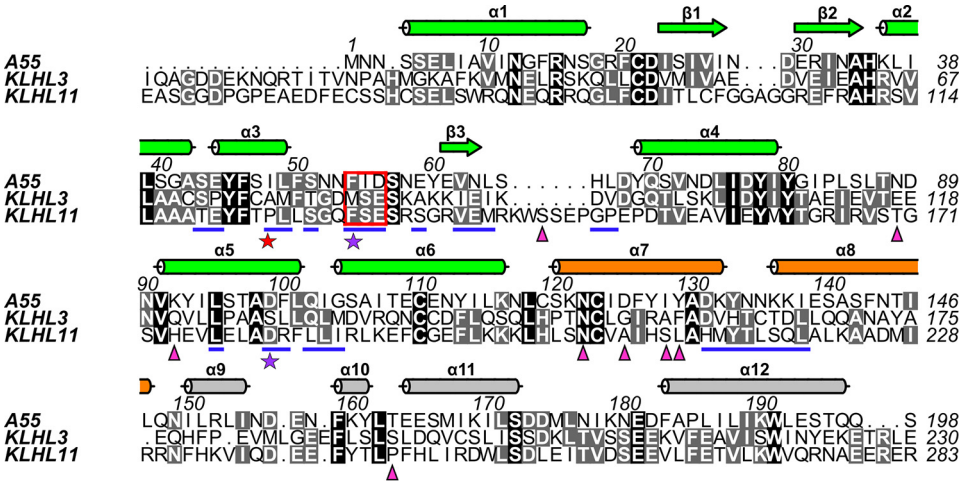

Figure 4. Structure-based sequence alignment of the A55, KLHL3, and KLHL11 BB domains. Columns are *shaded* based on amino acid similarity. Secondary structural elements for A55 are shown *above* the aligned sequences and colored as in Fig. 3*A*. Residues at the A55/Cul3 interface are *underlined in blue*. Residues selected for subsequent mutagenesis studies of A55 are marked by *stars* at bottom: the two conserved sites (Phe-54 and Asp-56) are marked by *purple stars*, and the nonconserved site (Ile-48) is marked by a *red star*. Residues from KLHL11 that are involved in Cul3–NTE binding are marked by *magenta triangles*.

Overall, the A55BB/Cul3NΔ22 complex closely resembles other structures of Cul3 in complex with cellular BTB domain–containing proteins (Fig. 3*C*). The A55-binding interface of Cul3–NTD is formed primarily of residues in helices α2 and α5, with extra contacts from the α1–α2 loop and from the C terminus of α3. Residues at the Cul3-binding interface of A55BB are primarily found in the BTB domain with additional contacts in the three-box region; the BACK domain does not contribute to the interaction (Fig. 4). This mode of interaction is consistent with the KLHL3/Cul3 (7), KLHL11/Cul3 (6), and KEAP1/Cul3

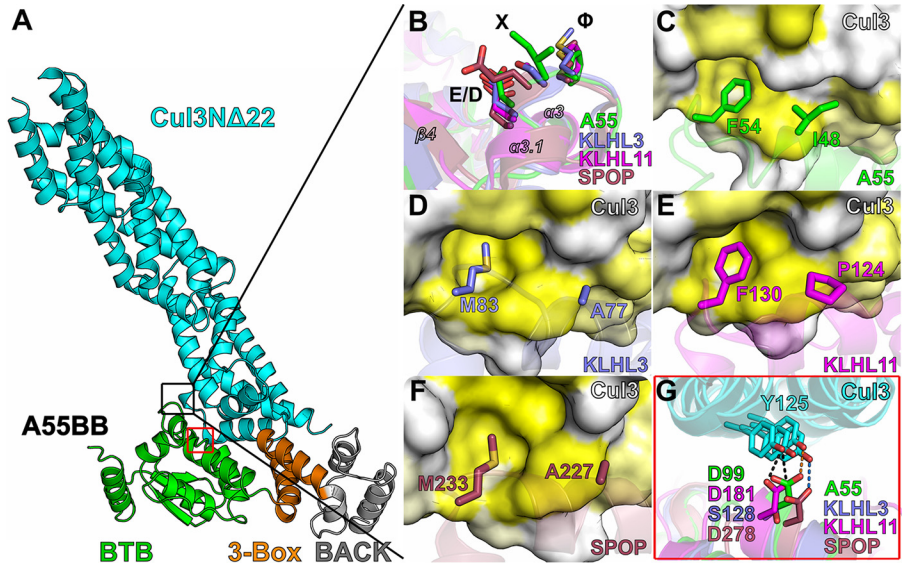

Figure 5. Conserved and nonconserved interactions at the interface between A55 and Cul3. *A,* A55BB/Cul3NΔ22 complex structure with two key Cul3-binding sites in the BTB domain boxed in *black* (enlarged in *B–F*) and *red* (enlarged in *G*). *B,* structural overlay of the ϕX(D/E) motifs from A55, KLHL3, KLHL11, and SPOP. *C–F,* surface of Cul3 colored by residue hydrophobicity from *yellow* (hydrophobic) to *white* (polar) (70). Hydrophobic binding pockets are shown for Phe-54 of A55, Met-83 of KLHL3, Phe-130 of KLHL11, and Met-233 of SPOP, which are equivalent to the ϕ residue of the ϕX(D/E) motif, and for Ile-48 of A55 and its equivalent residues Ala-77, Pro-124, and Ala-227 in KLHL3, KLHL11, and SPOP, respectively. *G,* overlay of the hydrogen bond formed between Tyr-125 of Cul3 and Asp-99 of A55 with equivalent residues Ser-128, Asp-181, and Asp-278 in KLHL3, KLHL11, and SPOP, respectively.

(PDB code 5NLB) complex structures (Fig. S2). Analyses of the interface areas and the number of interface residues for A55 and all available BTB/Cul3 complex structures showed no striking overall differences (Fig. S2). However, compared with other BTB/Cul3–NTD structures, the A55BB/Cul3 interface has more hydrogen bonds and a reduced contribution from hydrophobic interactions (Fig. S2).

Only 196 of the 250-aa residues that comprise A55BB could be modeled confidently; the density for side chains in the last modeled helix of the BACK domain (α10, residues 180–196) is weak compared with density for side chains at the BTB/Cul3 interface (Fig. S3, *A* and *B*), and density for BACK domain residues 197–250 was not sufficiently well resolved to be modeled unambiguously (Fig. S3*C*). Correspondingly, the B factors of A55 residues at the Cul3-binding interface are lower than in the BACK domain (Fig. S3*D*). Inspection of the crystal lattice shows large solvent channels next to the BACK domain, and this lack of crystal contacts at the C terminus is likely to account for the poor density observed in this region (Fig. S3, *C* and *E*). When superimposing KLHL11 and KLHL3 onto different regions of A55, inter-domain flexibility is evident (Fig. S4, *A–D* and *E–F*, respectively). Two pivot points in the structure can be found: the $BTB_{\alpha5-\alpha6}$ helix–turn–helix and the three-box region, respectively; the latter appears to be the major pivot point around which the BTB and BACK domain rotate relative to each other (Fig. S4, *I–K*). When measuring the angles between different subdomains ($BTB_{\alpha1-4}$, $BTB_{\alpha5-\alpha6}$, three-box, and BACK), the angle formed by $BTB_{\alpha5-\alpha6}$–three-box–BACK in A55 is much larger compared with the corresponding angles in KLHL3 and KLHL11, thus rendering A55 more linear across the BB domain than KLHL3 and KLHL11 (Fig. S4, *I–K*).

Crystals of the A55BB/Cul3NΔ22 could be obtained only when the A55BB protein had been methylated *in vitro*. Although there was density consistent with the presence of additional atoms adjacent to the amino groups of two lysine side chains (Lys-36 and Lys-132), they were not sufficiently well resolved to allow modeling of the methyl groups (Fig. S5*A*). Only one lysine (Lys-136) was found at the binding interface (Fig. S5*B*), and ITC studies showed that methylated A55BB binds to Cul3 with affinity similar to unmodified A55BB (Fig. S5, *C* and *D*).

Hydrophobic interaction at A55 residue 48 is required for high-affinity binding to Cul3

Despite similarity in the overall structures, A55BB binds Cul3–NTD with much higher affinity than other BTB proteins. It has been suggested the key determinant for the interaction with Cul3 is a conserved ϕX(D/E) motif found in the α3–β4 loops of the BTB domain, where ϕ is a hydrophobic residue, and X is any residue (6, 7, 13). This motif exists in A55, corresponding to residues Phe-54 (ϕ), Ile-55 (X), and Asp-56 (D/E), respectively (Figs. 4 and 5*B*). As in KLHL3, KLHL11, and SPOP, the side chain of residue ϕ (Phe-54) in A55 is buried in a hydrophobic cavity on the surface of Cul3 (Fig. 5, *C–F*). Mutation of the ϕ residue in SPOP to a charged residue (M233E) completely abolished binding to Cul3, highlighting the significance of the ϕ residue for the interaction (13). An F54E mutant of A55BB was purified and shown to have similar thermal stability to the WT protein (Fig. 6, *A* and *B*). ITC analysis demonstrated that the F54E mutation reduces the affinity of A55BB for Cul3NΔ22 and Cul3N by at least 10-fold compared with the WT protein, yielding dissociation constants (K_D) similar to those of cellular BTB proteins (Fig. 6, *C* and *D*; Table 3). This suggests that ϕ residue Phe-54 of A55 is involved in the interaction but is not critical for binding to Cul3. The A55 residue Asp-56, equivalent to the D/E residue of the ϕX(D/E) motif, forms side chain and backbone hydrogen bonds with Cul3 residues Ser-53 and Phe-54, respectively. A D56A mutation was introduced into A55, but the

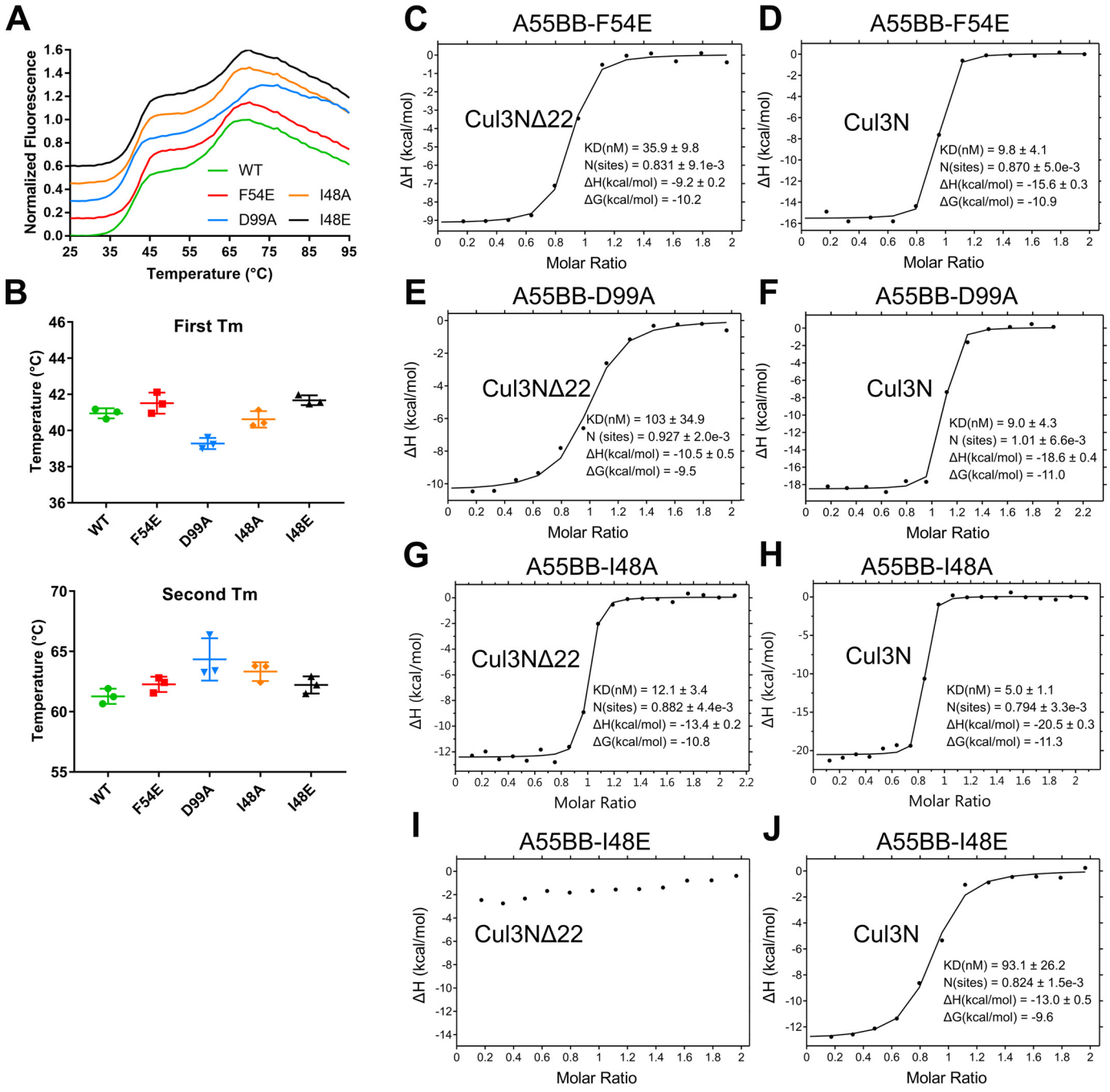

Figure 6. I48E mutation significantly impairs A55 binding to Cul3. *A,* representative thermal melt curves of WT A55BB and mutants F54E, D99A, I48A, and I48E from DSF studies. Curves are offset along the *vertical axis* for clarity. All experiments were performed in triplicate. *B,* comparison of the melting temperatures for WT A55BB (*green*), F54E (*red*), D99A (*blue*), I48A (*orange*), and I48E (*black*) mutants. *Upper* and *lower panels* display T_m values for the first and second melting events, respectively. *Error bars* show the standard errors of the mean from experiments performed in triplicate. *C–J,* representative ITC titration curves showing binding of A55BB mutants F54E (*C* and *D*), D99A (*E* and *F*), I48A (*G* and *H*), and I48E (*I* and *J*) to Cul3NΔ22 and Cul3N, respectively. Integrated changes in enthalpy (Δ*H*) are plotted against molar ratio of titrant. The corresponding dissociation constant (K_D), number of binding sites (*N*), enthalpy change (Δ*H*), and change in Gibbs free energy (Δ*G*) for each representative experiment are shown. All experiments were performed at least twice independently. Raw data for *C–J* are shown in Fig. S7.

mutant could not be purified following bacterial expression, suggesting Asp-56 is critical for the correct folding of A55.

As the ϕX(D/E) motif was not absolutely required for binding of A55 to Cul3, the contribution of other residues was investigated. A hydrogen bond is formed between Asp-99 of A55 and Tyr-125 of Cul3, and this interaction is conserved in KLHL11 and SPOP but not in KLHL3 (Fig. 5*G*). Mutation at this site only caused moderate reduction in affinities for both Cul3NΔ22 and Cul3N (Fig. 6, *E* and *F*). Residue Ile-48 of A55 is adjacent to the ϕ residue Phe-54 and, like Phe-54, the side chain of Ile-48 extends into a hydrophobic cleft on the Cul3 surface (Fig. 5*C*). This residue is not conserved in KLHL3, KLHL11, or SPOP, and the equivalent residues (Ala-77, Pro-124, and Ala-227, respectively) have smaller side chains and form less extensive interactions (Fig. 5, *D–F*). Two mutant forms of A55BB were generated, A55BB-I48E and A55BB-I48A, and both were

Table 3
Comparison of the dissociation constants (K_D) for WT and mutant A55BB for Cul3
Experiments were performed *n* times and the mean ± S.E. is shown.

Protein	Cul3NΔ22	Cul3N
	*n*M	*n*M
WT	5.3 ± 2.9 (*n* = 6)	<1 (*n* = 6)
F54E	54.7 ± 18.8 (*n* = 2)	12.0 ± 2.2 (*n* = 2)
D99A	119.0 ± 16.0 (*n* = 2)	5.4 ± 3.7 (*n* = 2)
I48A	9.5 ± 1.3 (*n* = 5)	3.2 ± 0.9 (*n* = 3)
I48E	ND[a] (*n* = 2)	73.8 ± 10.3 (*n* = 3)

[a] ND = none detected.

shown to have similar thermal stability to the WT protein (Fig. 6, *A* and *B*). A55BB-I48A retained high affinity for Cul3NΔ22 and Cul3N (Fig. 6, *G* and *H*). However, the I48E substitution reduced Cul3NΔ22 binding to levels undetectable by ITC and reduced the affinity for Cul3N by at least 2 orders of magnitude (Fig. 6, *I* and *J*), to well-below those of the cellular BTB proteins for Cul3–NTD (Tables 1 and 3). The residual binding of A55BB-I48E to Cul3N is likely to be mediated via contacts with Cul3N–NTE, as has been characterized previously for KLHL11 (6).

Discussion

An interaction between a poxvirus BTB–Kelch protein and Cul3 has been demonstrated previously for the ECTV protein EVM150 by co-immunoprecipitation from transfected cells (42, 43). Cellular BTB proteins have been reported to bind directly to Cul3 (6–8, 13, 24, 25, 33). However, because of the low sequence identity (20–25%) between poxvirus and cellular BTB proteins (Fig. 4), it was unclear whether EVM150 and other poxvirus BTB–Kelch proteins would bind Cul3 in a similar manner. Here, we show that VACV BTB–Kelch protein A55, a close orthologue of EVM150, also binds to Cul3, and this interaction is direct in nature. Surprisingly, the binding of Cul3 to A55BB is much tighter than to human BTB domains (Fig. 2 and Table 1). To understand the molecular basis of this tight interaction, the crystal structure of the A55BB/Cul3NΔ22 complex was determined using anisotropic diffraction data extending to 2.3 Å (with an observation/parameter ratio equivalent to that of an isotropic 2.8 Å resolution structure). This is the first reported crystal structure of a virus BTB–Kelch protein in complex with the E3 ubiquitin ligase scaffold protein Cul3.

The overall conformation of the A55BB/Cul3–NTD complex resembles closely the structures of other cellular BTB/Cul3–NTD protein complexes, with a similar mode of dimerization and a conserved Cul3-binding interface despite low sequence identities (Fig. 3, *C–E*; Fig. S2). The interface area and the number of interface residues at the A55BB/Cul3NΔ22-binding interface are comparable with cellular BTB/Cul3–NTD interfaces (Fig. S2, *inset table*). The conserved ϕX(D/E) motif, which was found to be a key contributor to the interaction between SPOP and Cul3, is conserved in A55 (Figs. 4 and 5*B*) (13). However, mutation of Phe-54 to glutamate at the ϕ position in A55BB only moderately reduced its affinity for Cul3 (Fig. 6, *C* and *D*), whereas the equivalent mutation in SPOP resulted in complete loss of binding (13). A55 residue Ile-48, adjacent to Phe-54, makes more extensive contacts with Cul3 than the equivalent residues in cellular BTB proteins (Fig. 5, *C–F*). Substitution of Ile-48 to alanine caused only a modest decrease in affinity (Table 3), demonstrating that the additional hydrophobic interactions mediated by isoleucine at this position are not the sole determinants of higher-affinity Cul3 binding by A55BB. However, substitution of Ile-48 to glutamate weakened the interaction with the Cul3 N-terminal domain lacking the NTE (Cul3NΔ22) such that it could no longer be detected by ITC, and reduced the affinity for the full Cul3 N-terminal domain (Cul3N) by at least 2 orders of magnitude (Fig. 6, *G* and *H*; Table 3). An equivalent mutation (A77E) in KLHL3 similarly reduced the affinity for Cul3NΔ20 to levels undetectable by ITC (7). Taken together, these results confirm that hydrophobic interactions at this position, adjacent to the conserved ϕX(D/E) motif, are necessary for binding of BTB proteins to Cul3. Interestingly, ITC studies suggest that the A55BB/Cul3–NTD interaction is more entropically favorable than the KLHL3-BB/Cul3–NTD interaction (Fig. 2 and Table 1), whereas structural analysis suggests that hydrophobic interactions contribute less energy (via the entropically-favorable release of solvent) to the A55/Cul3 interaction (Fig. S2, *inset table*). In Cul3-bound KLHL3, KLHL11, and SPOP structures, the $\alpha3$–$\beta4$ loops, which contain the ϕ residue and interact with hydrophobic pockets on the Cul3 surface, adopt helical conformations (*helix α3.1*, Fig. 5, *B* and *D–F*). In A55, the ϕ residue Phe-54 also fits into a deep hydrophobic pocket on the surface of Cul3, but the $\alpha3$–$\beta4$ loop of A55 does not adopt a helical conformation (Fig. 5, *A* and *C*). Interestingly, in the structures of unbound KLHL11 and SPOP, the $\alpha3$–$\beta4$ loop containing the ϕ residue is less well ordered and has a different conformation (6, 8). Such structural rearrangement upon binding to Cul3 would present an entropic penalty to binding. It is tempting to speculate that a lack of such a $\alpha3$–$\beta4$ loop rearrangement, rather than the burial of exposed hydrophobic regions, contributes to the entropically-favorable tight binding of A55BB to Cul3–NTD. Furthermore, such structural rearrangement may not occur in the absence of the favorable hydrophobic interaction mediated by the ϕ residue, suggesting a mechanism by which binding to Cul3 would be more significantly diminished for SPOP than for A55 when this residue was mutated.

Sequence alignments reveal the BB domains of A55 and other orthopoxvirus BTB–Kelch orthologues such as EVM150 to share extensive (>77%) identity (Table 4), including conservation of the residues in the ϕX(D/E) motif and Ile-48 (Fig. 7). This strongly suggests that the interaction between A55 orthologues and Cul3 is conserved among poxviruses. In contrast, most of the Cul3-binding residues of A55 are not conserved in the other two VACV BTB–Kelch proteins, C2 and F3 (Fig. 7), which share little sequence identity to A55 (25 and 23%, respectively). This suggests that these proteins are unlikely to interact with Cul3, despite being classified as BTB–Kelch proteins, and is consistent with these proteins being functionally distinct (4, 31, 32). The N-terminal dimerization helix of the BTB domain appears to be missing in C2 (Fig. 7) suggesting that, unlike most BTB–Kelch proteins, C2 may not be able to form homo- or heterodimers via the same mechanism as A55.

In vivo, VACV expressing A55 induced a smaller lesion in a murine model of intradermal infection compared with a virus lacking A55 (4). In cells, the BTB domain of the ECTV EVM150

ASBMB

Table 4
Sequence identities between A55BB and the BB domains of poxvirus orthologues and VACV paralogues C2 and F3

	Ectromelia EVM150	Cowpox A57	Skunkpox WA-176	Raccoonpox Herman-172	Volepox CA-176	VACV C2	VACV F3
VACV A55	95%	98%	79%	77%	75%	25%	23%

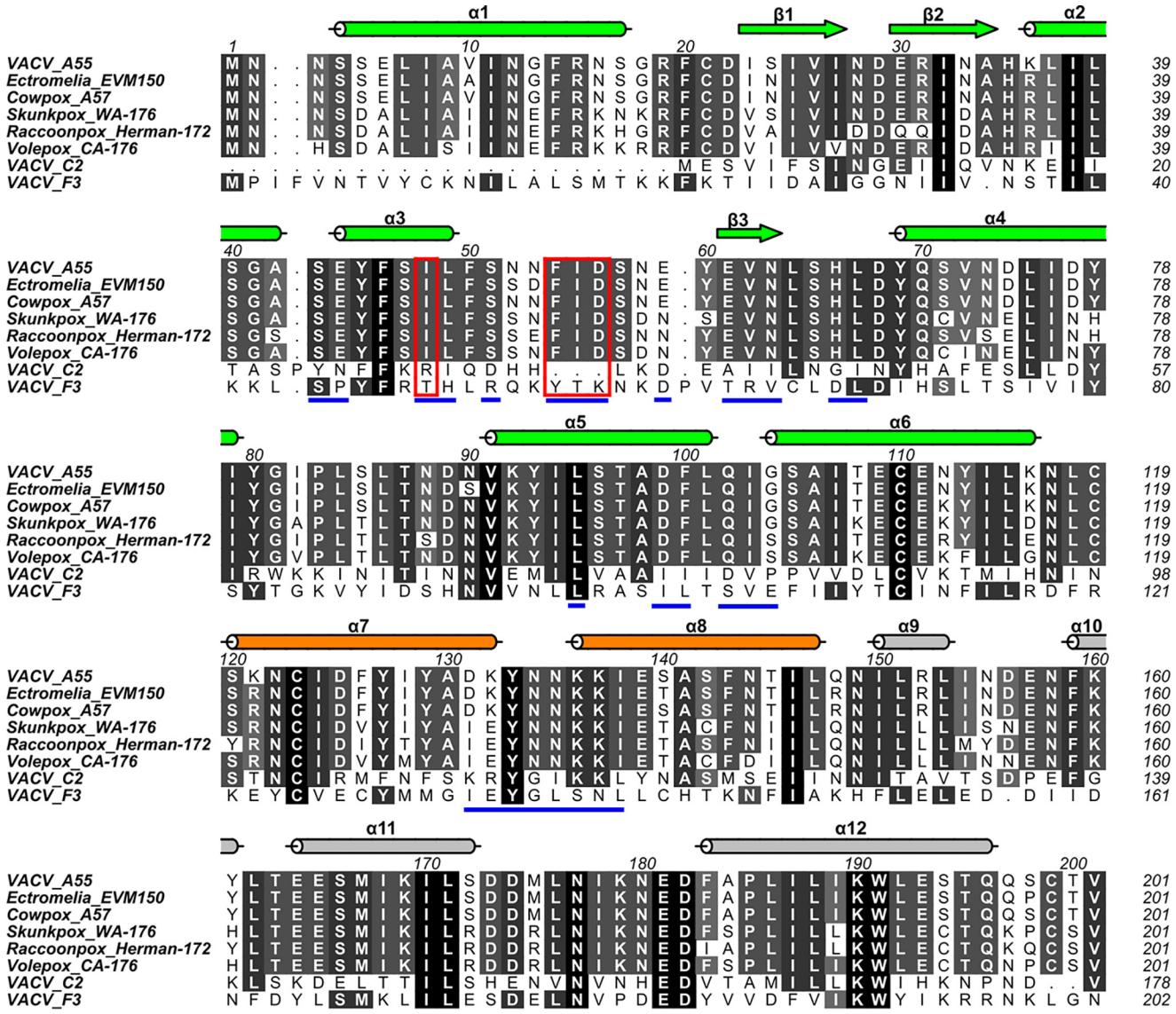

Figure 7. Cul3-binding residues of A55 are conserved across orthopoxvirus orthologues but not in VACV paralogues C2 and F3. Multiple sequence alignment of the A55 BB domains against its orthologues from selected poxviruses and two other VACV BTB–Kelch proteins, C2 and F3. Columns are *shaded* based on amino acid similarity. Secondary structural elements for A55 are shown *above* the aligned sequences and colored as in Fig. 3*A*. Residues at the A55/Cul3 interface are *underlined in blue*. Residues aligned with A55-Ile-48 and the *ϕX*(D/E) motif are *boxed in red*.

was reported to inhibit TNFα-induced NF-κB activation; however, this inhibition appears to be Cul3-independent (42). The interaction between A55 and Cul3 therefore is unlikely to be relevant for the inhibition of NF-κB signaling. As a scaffold protein for an E3 ubiquitin ligase complex, Cul3 not only interacts with the BTB–Kelch family of adaptor proteins but also other BTB domain–containing adaptor proteins such as BTB zinc-finger proteins, MATH-BTB proteins (where MATH is Meprin and TRAF homology domain), small RhoBTB GTPases, and KCTD proteins (5, 8, 10, 13, 20, 24, 52). The outcome of the interaction will depend on the specific substrates recruited by the BTB adaptor proteins and will regulate a diverse range of cellular processes, including hypoxic response, ion-channel gating, as well as cytoskeleton organization (19, 53, 54). The fact that A55BB is able to bind Cul3–NTD with much stronger affinity than reported, cellular binding partners suggest two possible functions of A55. First, A55 may bind to Cul3 and redirect the E3 ubiquitin ligase complex to ubiquitylate otherwise untargeted proteins for proteasomal degradation. Alternatively, A55 may sequester Cul3 and prevent the ubiquitylation and/or proteasomal degradation of proteins that are normally ubiquitylated/degraded upon viral infection. Further experiments are required to discriminate whether A55 fulfills either or both of these roles during infection.

A55BB binding to the Cul3 N-terminal domain is significantly increased by the presence of the N-terminal 22 amino acids of Cul3 (Table 1), and the I48E mutant lacks the ability to bind Cu3NΔ22 yet can bind Cul3N with nanomolar affinity (Table 3). This NTE of Cul3 has been shown to interact extensively with a hydrophobic groove formed primarily by the three-box region of KLHL11 (Fig. S6*A*) (6). Comparison of the structures of KLHL11 in complex with Cul3N or Cul3NΔ22 shows this groove to be pre-formed, rather than being induced by NTE binding (Fig. S6, *A* and *B*). However, sequence and structural alignment of A55 and KLHL11 suggest that an equivalent hydrophobic groove is not present on the surface of A55 (Fig. 4 and Fig. S6*C*). Indeed, the BTB, three-box, and BACK domains are arranged in linear fashion in A55, whereas they form a crescent in KLHL11 or KLHL3 (Fig. S4, *I–K*). It is therefore likely that A55 binds the Cul3–NTE via a different set of interactions. Crystallization trials of A55 with Cul3 containing the NTE region (Cul3N) have to date been unsuccessful, and further studies are thus needed to identify residues key for the interaction between A55 and the Cul3–NTE.

Conclusion

The structure of the first virus BTB–Kelch protein in complex with Cul3 is presented here, which has provided insight into how poxviruses may utilize the host Cul3-based E3 ubiquitin ligase complex for its own benefit. A55 binds Cul3 with much stronger affinity than cellular BTB–Kelch proteins. A single point mutation in A55, I48E, significantly diminishes Cul3 binding and could be exploited by future studies to probe the contribution of the A55–Cul3 interaction to VACV virulence.

Experimental procedures

Construct design

Codon-optimized VACV strain Western Reserve (WR) gene *A55R* (Uniprot P24768) full length, *A55R* BTB (residues 1–250), and *A55R* Kelch (residues 251–565) or VACV WR *B14R* (Uniprot P24772) were subcloned into pCDNA4/TO for inducible expression in mammalian cells with an N- or C-terminal STREPI and STREPII tag followed by FLAG tag (TAP), respectively. The mammalian expression vectors pcDNA-myc-*CUL3* (19893) and pcDNA-myc-*CUL5* (19895) were purchased from Addgene. The sequence encoding the A55 BB domain of the VACV strain WR (residues 1–250) was codon-optimized for expression in mammalian cells and cloned into the pOPTnH vector (55) for expression in *Escherichia coli* with a C-terminal Lys–His_6 tag. Human Cul3NΔ22 (Uniprot Q13618, residues 23–388) and Cul3N (Uniprot Q13618, residues 1–388) with the I342R and L346D stabilizing mutations (6) in pNIC-CTHF with C-terminal TEV-cleavable His_6 tags were a gift from Nicola Burgess-Brown (Addgene plasmids 53672 and 53673). KLHL3 (Uniprot Q9UH77, residues 24–276) cloned into pMCSG7 with an N-terminal TEV-cleavable His_6 tag was a gift from Alan X. Ji and Gilbert G. Prive (7). QuikChange mutagenesis PCR (Agilent) was used to generate the A55-F54E, A55-D56A, A55-D99A, A55-I48A, and A55-I48E mutants as per the manufacturer's protocol.

Immunoprecipitation

HEK293T–REx (Invitrogen) cells were maintained in Dulbecco's modified minimal essential medium (DMEM; Gibco) supplemented with 10% fetal bovine serum (Pan Biotech), nonessential amino acids (Gibco), and 50 μg/ml penicillin/streptomycin (Gibco) at 37 °C in a 5% CO_2 atmosphere. HEK293T–Rex-inducible cell lines were constructed following transfection with the pCDNA4/TO expression plasmids described above using LT1 transfection reagent following the manufacturer's instructions (MirusBio). Transfected cells were selected and maintained in DMEM supplemented with 10 μg/ml blasticidin and 100 μg/ml Zeocin, following the manufacturer's instructions (Invitrogen). B14–TAP, TAP–A55, TAP–A55–BTB (TAP–A55BB), or TAP–A55-Kelch HEK293T–REx cells were induced for 24 h with 2 μg/ml doxycycline, washed in ice-cold phosphate-buffered saline (PBS), and subsequently were lysed in either 0.5% Nonidet P-40 (IGEPAL CA-630) in PBS supplemented with protease inhibitor or RIPA buffer (50 mM Tris, pH 8.0, 1% Nonidet P-40, 150 mM NaCl, 0.5% sodium deoxycholate, 0.5 mM EDTA, 0.1% SDS supplemented with protease inhibitor) where stated. Lysates were cleared at 15,000 × *g* at 4 °C, and proteins were immunoprecipitated at 4 °C overnight with FLAG M2 beads or Fastflow G–Sepharose (GE Healthcare) incubated previously with mouse monoclonal anti-Myc clone 9B11 (CST catalog no. 2276) at 1:50 dilution. Beads were washed three times in 1 ml of lysis buffer by centrifugation for 1 min at 8,000 × *g*. After the final wash, beads were incubated in 4× sample loading dye (0.5 M Tris, pH 6.8, 40% glycerol, 6% SDS, 1% bromphenol blue, and 0.8% β-mercaptoethanol), boiled, and analyzed by immunoblotting.

Protein expression and purification

WT and mutant A55BB and Cul3NΔ22 were expressed in B834(DE3) *E. coli* cells (Novagen), and Cul3N and KLHL3 were expressed in Rosetta2(DE3)pLysS *E. coli* cells (Novagen). Bacteria were grown at 37 °C in 2× TY medium with shaking at 200 rpm to an A_{600} of 0.7–0.9, whereupon protein expression was induced by either adding 0.2 mM IPTG and incubating at 37 °C for 4 h (Cul3N) or by cooling the cultures to 22 °C, adding 0.2 mM IPTG, and incubating for 4 h (Cul3NΔ22) or overnight (WT and mutant A55). Cells were harvested by centrifugation at 5,000 × *g* for 15 min, and pellets were stored at −80 °C.

Cells were thawed and resuspended in lysis buffer containing 20 mM HEPES, pH 7.5, 500 mM NaCl, 1 mM β-mercaptoethanol, 0.05% Tween 20, 0.5 mM $MgCl_2$, 400 units of bovine DNase I (Roche Applied Science), and 200 μl of EDTA-free protease inhibitor mixture (Sigma). Cells were lysed by passage through a TS series cell disruptor (Constant Systems) at 24,000 p.s.i. Lysates were collected and cleared by centrifugation at 40,000 × *g* for 30 min at 4 °C. Cleared lysates were applied to a 5-ml HiTrap TALON crude column (GE Healthcare) pre-equilibrated with binding buffer (20 mM HEPES, pH 7.5, 500 mM NaCl, 5 mM β-mercaptoethanol) to capture the His_6-tagged proteins. The column was washed with binding buffer, and the bound proteins were eluted with a gradient of 10–150 mM imidazole in binding buffer. Eluted proteins were pooled, concentrated,

and further purified by SEC using a Superdex 200 column (GE Healthcare) equilibrated in gel-filtration buffer (20 mM HEPES, pH 7.5, 200 mM NaCl, 1 mM DTT). For Cul3N, an additional anion-exchange chromatography purification step was performed by exchanging the protein into 20 mM Tris, pH 7.5, 10 mM NaCl, 1 mM DTT and applying to a Mono Q 5/50 GL column (GE Healthcare) before eluting with a linear gradient of NaCl (10 mM to 1 M). Purified proteins were concentrated, snap-frozen in liquid nitrogen, and stored at −80 °C. A55BB migrates more rapidly than expected in SDS-PAGE; peptide mass fingerprinting was used to confirm the identity and integrity of the purified protein.

Size-exclusion chromatography coupled to multiangle light scattering (SEC-MALS)

SEC-MALS experiments were performed at room temperature. For each experiment, 100 μl of protein at 3 mg/ml was injected onto a Superdex 200 increase 10/300 GL column (GE Healthcare) pre-equilibrated with 20 mM HEPES, 150 mM NaCl, and 2 mM DTT at a flow rate of 0.5 ml/min. The static light scattering, differential refractive index, and the UV absorbance at 280 nm were measured in-line by DAWN 8+ (Wyatt Technology), Optilab T-rEX (Wyatt Technology), and Agilent 1260 UV (Agilent Technologies) detectors. The corresponding molar mass from each elution peak was calculated using ASTRA 6 software (Wyatt Technology).

ITC

ITC experiments were carried out at 25 °C on an automated MicroCal PEAQ-ITC (Malvern Panalytical). Proteins were exchanged into gel-filtration buffer (20 mM HEPES, 200 mM NaCl, 1 mM DTT) either by SEC or extensive dialysis prior to experiments. Titrants (WT and mutant A55 and KLHL3) at concentrations between 70 and 100 μM were titrated into 7 μM titrates (Cul3NΔ22 or Cul3N) either as 19 × 2-μl injections (WT A55, I48E mutant and KLHL3) or 13 × 3-μl injections (mutant A55 except I48E). Data were analyzed using the MicroCal PEAQ-ITC analysis software (Malvern Panalytical) and fitted using a one-site binding model.

Reductive methylation

Reductive methylation was carried out at 4 °C using modified protocols from Walter *et al.* (46). Purified A55BB was diluted to 0.8 mg/ml and dialyzed into buffer containing 50 mM HEPES, pH 7.5 and 250 mM NaCl. The protein was mixed with 20 μl/ml of 1 M dimethylamine/borane complex (Sigma) and 40 μl/ml of 1% formaldehyde (UltraPure EM grade, Polysciences) and incubated for 2 h at 4 °C. This step was repeated once before mixing with an additional 10 μl/ml of 1 M dimethylamine/borane complex and incubating overnight at 4 °C. The reaction was quenched with 10 μl of 1 M Tris, pH 7.5. Methylated A55BB was further purified by SEC using a Superdex 200 10/300 GL column equilibrated in 20 mM Tris, pH 7.5, 200 mM NaCl, and 1 mM DTT before being concentrated, snap-frozen, and stored at −80 °C.

Isoelectric focusing (IEF) gel analysis

The IEF gel analysis was performed at 4 °C using a Novex pH 3–7 IEF gel (ThermoFisher Scientific) according to the manufacturer's instructions. Native and methylated A55BB were diluted with MilliQ water to 0.8 mg/ml in a total volume of 5 μl and mixed with an equal volume of 2× Novex pH 3–10 IEF sample buffer (ThermoFisher Scientific) before loading onto the IEF gel. The gel was fixed in 12% TCA for 30 min and washed with MilliQ water before staining with InstantBlue Protein Stain (Expedeon).

Differential scanning fluorimetry (DSF)

DSF experiments were performed in 96-well PCR microplates (Axygen Scientific) on a ViiA 7 real-time PCR machine (Life Technologies, Inc.). To each well of the plate, buffer (20 mM HEPES, 200 mM NaCl, 1 mM DTT), protein, and 10× protein thermal shift dye (Applied Biosystems) were mixed at 8:1:1 volume ratio in a final volume of 20 μl and a protein concentration of 0.2 μg/μl. Samples were subjected to thermal denaturation from 25 to 95 °C with 1 °C increments per 20 s, and real-time fluorescence was recorded. Normalized melt curves were fitted to a biphasic sigmoidal curve using Prism7 (GraphPad Software), and the melting temperatures (T_m) were taken as mid-points of the sigmoids.

Crystallization and data collection

Methylated A55BB was mixed with Cul3NΔ22 at 1:1 molar ratio, and the complex was purified by SEC using a Superdex 200 10/300 GL column (GE Healthcare) in 20 mM Tris, pH 7.5, 200 mM NaCl, 1 mM DTT. The purified complex was concentrated to 16.3 mg/ml, and sitting-drop vapor diffusion experiments were attempted by mixing 100 nl of protein with 100 nl of reservoir (4% (v/v) tacsimate, pH 6.5, 12% (w/v) PEG3350) and equilibrating against 80 μl of the reservoir solution at 20 °C. Thin needles were observed after 2 weeks. Varying the pH, concentration of the tacsimate, concentration of PEG3350, and the protein/reservoir ratio in the sitting drops gave rise to larger crystals that diffracted to ~3.8 Å on Diamond beamline I03. For further optimization, seed stocks for microseeding were generated as described previously (56). Briefly, crystals were crushed and transferred into 50 μl of stabilizing solution (original reservoir solution) and vortexed, and seven 5-fold serial dilutions of seed into stabilizing solution were generated. Sitting drops were prepared using 100 nl of protein, 150 nl of reservoir, and 50 nl of seed stock. Eventually, a drop containing 3.29% (v/v) tacsimate, pH 6.5, 9.92% (w/v) PEG3350, and 50 nl of 625-fold diluted seed stock gave rise to crystals that diffracted to 2.3 Å in the best direction on Diamond beamline I04. The crystals were cryoprotected by briefly sweeping through reservoir solution containing 25% (v/v) glycerol and flash-cryocooled by plunging into liquid nitrogen. Diffraction data were collected at 100 K on the Diamond beamline I04. Data were indexed and integrated using DIALS (57) as implemented by the xia2 processing pipeline (58). Because of severe anisotropic diffraction, diffraction data were subject to anisotropic scaling using STARANISO (47) and AIMLESS (59).

Structure determination

The structure of the A55BB(M)/Cul3NΔ22 complex was solved by molecular replacement using PHENIX PHASER-MR (60). An initial search using each domain of the SPOP/Cul3 complex (13) (PDB code 4EOZ) as search models successfully placed one copy of Cul3NΔ22, but no solution corresponding to A55BB was forthcoming. MOLREP (61) from the CCP4 pro-

gram suite (62) was used to locate the A55 BTB domain using B-Cell Lymphoma 6 BTB Domain (49) (PDB code 1R29) as a search model. The three-box region and the first four helices of the A55 BACK domain (α9–α12) were manually built using COOT (63) with iterative rounds of refinement using Refmac5 (64). The structure was improved by the use of real-time molecular dynamics-assisted model building and map fitting with the program ISOLDE (50), followed by TLS and positional refinement using BUSTER (51). The quality of the model was monitored throughout the refinement process using Molprobity (65).

Bioinformatics and structural analysis

Multiple sequence alignments were performed using Clustal Omega (66) and annotated using ALINE (67). Analyses of the binding interfaces were performed using the PDBePISA webserver (68). Molecular figures were generated using PyMOL (69).

Author contributions—C. G. data curation; C. G., M. A. P., T. I. C., and S. C. G. investigation; C. G. and M. A. P. visualization; C. G., M. A. P., T. I. C., G. L. S., and S. C. G. methodology; C. G. and S. C. G. writing-original draft; C. G., M. A. P., T. I. C., G. L. S., and S. C. G. writing-review and editing; T. I. C. software; G. L. S. and S. C. G. conceptualization; G. L. S. and S. C. G. supervision; G. L. S. and S. C. G. funding acquisition; G. L. S. and S. C. G. project administration.

Acknowledgments—We thank the Diamond Light Source for access to beamlines I03 and I04 (mx8547), remote access to which was supported in part by the EU FP7 infrastructure Grant BIOSTRUCT-X (Contract No. 283570). We thank Janet Deane for assistance with SEC-MALS experiments and useful discussions. We thank Alan X. Ji and Gilbert G. Privé for sharing the pMCSG7-His-TEV-KLHL3 plasmid. We thank Nicola Burgess-Brown for sharing the pNIC-CTHF-Cul3NΔ22 and pNIC-CTHF-Cul3N plasmids via Addgene.

References

1. Fenner, F., Anderson, D. A., Arita, I., Jezek, Z., and Ladnyi, I. D. (1988) Smallpox and its eradication. World Health Organization, Geneva, Switzerland
2. Smith, G. L., Benfield, C. T., Maluquer de Motes, C., Mazzon, M., Ember, S. W., Ferguson, B. J., and Sumner, R. P. (2013) Vaccinia virus immune evasion: mechanisms, virulence and immunogenicity. *J. Gen. Virol.* **94,** 2367–2392 CrossRef Medline
3. Bahar, M. W., Graham, S. C., Chen, R. A., Cooray, S., Smith, G. L., Stuart, D. I., and Grimes, J. M. (2011) How vaccinia virus has evolved to subvert the host immune response. *J. Struct. Biol.* **175,** 127–134 CrossRef Medline
4. Beard, P. M., Froggatt, G. C., and Smith, G. L. (2006) Vaccinia virus kelch protein A55 is a 64-kDa intracellular factor that affects virus-induced cytopathic effect and the outcome of infection in a murine intradermal model. *J. Gen. Virol.* **87,** 1521–1529 CrossRef Medline
5. Pintard, L., Willems, A., and Peter, M. (2004) Cullin-based ubiquitin ligases: Cul3–BTB complexes join the family. *EMBO J.* **23,** 1681–1687 CrossRef Medline
6. Canning, P., Cooper, C. D., Krojer, T., Murray, J. W., Pike, A. C., Chaikuad, A., Keates, T., Thangaratnarajah, C., Hojzan, V., Ayinampudi, V., Marsden, B. D., Gileadi, O., Knapp, S., von Delft, F., and Bullock, A. N. (2013) Structural basis for Cul3 protein assembly with the BTB–Kelch family of E3 ubiquitin ligases. *J. Biol. Chem.* **288,** 7803–7814 CrossRef Medline
7. Ji, A. X., and Privé, G. G. (2013) Crystal structure of KLHL3 in complex with Cullin3. *PLoS ONE* **8,** e60445 CrossRef Medline
8. Zhuang, M., Calabrese, M. F., Liu, J., Waddell, M. B., Nourse, A., Hammel, M., Miller, D. J., Walden, H., Duda, D. M., Seyedin, S. N., Hoggard, T., Harper, J. W., White, K. P., and Schulman, B. A. (2009) Structures of SPOP–substrate complexes: insights into molecular architectures of BTB-Cul3 ubiquitin ligases. *Mol. Cell* **36,** 39–50 CrossRef Medline
9. Krek, W. (2003) BTB proteins as henchmen of Cul3-based ubiquitin ligases. *Nat. Cell Biol.* **5,** 950–951 CrossRef Medline
10. Stogios, P. J., Downs, G. S., Jauhal, J. J., Nandra, S. K., and Privé, G. G. (2005) Sequence and structural analysis of BTB domain proteins. *Genome Biol.* **6,** R82 CrossRef Medline
11. Xu, L., Wei, Y., Reboul, J., Vaglio, P., Shin, T. H., Vidal, M., Elledge, S. J., and Harper, J. W. (2003) BTB proteins are substrate-specific adaptors in an SCF-like modular ubiquitin ligase containing CUL-3. *Nature* **425,** 316–321 CrossRef Medline
12. Stogios, P. J., and Privé, G. G. (2004) The BACK domain in BTB-kelch proteins. *Trends Biochem. Sci.* **29,** 634–637 CrossRef Medline
13. Errington, W. J., Khan, M. Q., Bueler, S. A., Rubinstein, J. L., Chakrabartty, A., and Privé, G. G. (2012) Adaptor protein self-assembly drives the control of a cullin-RING ubiquitin ligase. *Structure* **20,** 1141–1153 CrossRef Medline
14. Zollman, S., Godt, D., Privé, G. G., Couderc, J. L., and Laski, F. A. (1994) The BTB domain, found primarily in zinc finger proteins, defines an evolutionarily conserved family that includes several developmentally regulated genes in *Drosophila*. *Proc. Natl. Acad. Sci. U.S.A.* **91,** 10717–10721 CrossRef Medline
15. Prag, S., and Adams, J. C. (2003) Molecular phylogeny of the kelch-repeat superfamily reveals an expansion of BTB/kelch proteins in animals. *BMC Bioinformatics* **4,** 42 CrossRef Medline
16. Xue, F., and Cooley, L. (1993) Kelch encodes a component of intercellular bridges in *Drosophila* egg chambers. *Cell* **72,** 681–693 CrossRef Medline
17. Robinson, D. N., and Cooley, L. (1997) *Drosophila* kelch is an oligomeric ring canal actin organizer. *J. Cell Biol.* **138,** 799–810 CrossRef Medline
18. Hudson, A. M., and Cooley, L. (2010) *Drosophila* Kelch functions with Cullin-3 to organize the ring canal actin cytoskeleton. *J. Cell Biol.* **188,** 29–37 CrossRef Medline
19. Dhanoa, B. S., Cogliati, T., Satish, A. G., Bruford, E. A., and Friedman, J. S. (2013) Update on the Kelch-like (KLHL) gene family. *Hum. Genomics* **7,** 13 CrossRef Medline
20. Chen, Y., Yang, Z., Meng, M., Zhao, Y., Dong, N., Yan, H., Liu, L., Ding, M., Peng, H. B., and Shao, F. (2009) Cullin mediates degradation of RhoA through evolutionarily conserved BTB adaptors to control actin cytoskeleton structure and cell movement. *Mol. Cell* **35,** 841–855 CrossRef Medline
21. Furukawa, M., and Xiong, Y. (2005) BTB protein Keap1 targets antioxidant transcription factor Nrf2 for ubiquitination by the Cullin 3-Roc1 ligase. *Mol. Cell. Biol.* **25,** 162–171 CrossRef Medline
22. Cullinan, S. B., Gordan, J. D., Jin, J., Harper, J. W., and Diehl, J. A. (2004) The Keap1-BTB protein is an adaptor that bridges Nrf2 to a Cul3-based E3 ligase: oxidative stress sensing by a Cul3-Keap1 ligase. *Mol. Cell. Biol.* **24,** 8477–8486 CrossRef Medline
23. Chen, H. Y., Liu, C. C., and Chen, R. H. (2016) Cul3-KLHL20 ubiquitin ligase: physiological functions, stress responses, and disease implications. *Cell Div.* **11,** 5 CrossRef Medline
24. Balasco, N., Pirone, L., Smaldone, G., Di Gaetano, S., Esposito, L., Pedone, E. M., and Vitagliano, L. (2014) Molecular recognition of Cullin3 by KCTDs: insights from experimental and computational investigations. *Biochim. Biophys. Acta* **1844,** 1289–1298 CrossRef Medline
25. Pinkas, D. M., Sanvitale, C. E., Bufton, J. C., Sorrell, F. J., Solcan, N., Chalk, R., Doutch, J., and Bullock, A. N. (2017) Structural complexity in the KCTD family of Cullin3-dependent E3 ubiquitin ligases. *Biochem. J.* **474,** 3747–3761 CrossRef Medline
26. Bardwell, V. J., and Treisman, R. (1994) The POZ domain: a conserved protein–protein interaction motif. *Genes Dev.* **8,** 1664–1677 CrossRef Medline
27. Raoult, D., Audic, S., Robert, C., Abergel, C., Renesto, P., Ogata, H., La Scola, B., Suzan, M., and Claverie, J. M. (2004) The 1.2-megabase genome sequence of mimivirus. *Science* **306,** 1344–1350 CrossRef Medline
28. Assis, F. L., Franco-Luiz, A. P. M., Dos Santos, R. N., Campos, F. S., Dornas, F. P., Borato, P. V. M., Franco, A. C., Abrahao, J. S., Colson, P., and Scola, B. (2017) Genome characterization of the first mimiviruses of lineage C isolated in Brazil. *Front. Microbiol.* **8,** 2562 CrossRef Medline
29. Suhre, K. (2005) Gene and genome duplication in *Acanthamoeba polyphaga* mimivirus. *J. Virol.* **79,** 14095–14101 CrossRef Medline

ASBMB

30. Saini, H. K., and Fischer, D. (2007) Structural and functional insights into mimivirus ORFans. *BMC Genomics* **8,** 115 CrossRef Medline
31. Pires de Miranda, M., Reading, P. C., Tscharke, D. C., Murphy, B. J., and Smith, G. L. (2003) The vaccinia virus kelch-like protein C2L affects calcium-independent adhesion to the extracellular matrix and inflammation in a murine intradermal model. *J. Gen. Virol.* **84,** 2459–2471 CrossRef Medline
32. Froggatt, G. C., Smith, G. L., and Beard, P. M. (2007) Vaccinia virus gene F3L encodes an intracellular protein that affects the innate immune response. *J. Gen. Virol.* **88,** 1917–1921 CrossRef Medline
33. Smaldone, G., Pirone, L., Balasco, N., Di Gaetano, S., Pedone, E. M., and Vitagliano, L. (2015) Cullin 3 recognition is not a universal property among KCTD proteins. *PLoS ONE* **10,** e0126808 CrossRef Medline
34. Furukawa, M., He, Y. J., Borchers, C., and Xiong, Y. (2003) Targeting of protein ubiquitination by BTB-Cullin 3-Roc1 ubiquitin ligases. *Nat. Cell Biol.* **5,** 1001–1007 CrossRef Medline
35. Mahon, C., Krogan, N. J., Craik, C. S., and Pick, E. (2014) Cullin E3 ligases and their rewiring by viral factors. *Biomolecules* **4,** 897–930 CrossRef Medline
36. Mercer, J., Snijder, B., Sacher, R., Burkard, C., Bleck, C. K., Stahlberg, H., Pelkmans, L., and Helenius, A. (2012) RNAi screening reveals proteasome- and Cullin3-dependent stages in vaccinia virus infection. *Cell Rep.* **2,** 1036–1047 CrossRef Medline
37. Rudnicka, A., and Yamauchi, Y. (2016) Ubiquitin in influenza virus entry and innate immunity. *Viruses* **8,** E293 Medline
38. Barry, M., van Buuren, N., Burles, K., Mottet, K., Wang, Q., and Teale, A. (2010) Poxvirus exploitation of the ubiquitin-proteasome system. *Viruses* **2,** 2356–2380 CrossRef Medline
39. Seissler, T., Marquet, R., and Paillart, J. C. (2017) Hijacking of the ubiquitin/proteasome pathway by the HIV auxiliary proteins. *Viruses* **9,** E322 Medline
40. Smith, M. C., Boutell, C., and Davido, D. J. (2011) HSV-1 ICP0: paving the way for viral replication. *Future Virol.* **6,** 421–429 CrossRef Medline
41. Lanfranca, M. P., Mostafa, H. H., and Davido, D. J. (2014) HSV-1 ICP0: an E3 ubiquitin ligase that counteracts host intrinsic and innate immunity. *Cells* **3,** 438–454 CrossRef Medline
42. Wang, Q., Burles, K., Couturier, B., Randall, C. M., Shisler, J., and Barry, M. (2014) Ectromelia virus encodes a BTB/kelch protein, EVM150, that inhibits NF-κB signaling. *J. Virol.* **88,** 4853–4865 CrossRef Medline
43. Wilton, B. A., Campbell, S., Van Buuren, N., Garneau, R., Furukawa, M., Xiong, Y., and Barry, M. (2008) Ectromelia virus BTB/kelch proteins, EVM150 and EVM167, interact with cullin-3-based ubiquitin ligases. *Virology* **374,** 82–99 CrossRef Medline
44. Chen, R. A., Ryzhakov, G., Cooray, S., Randow, F., and Smith, G. L. (2008) Inhibition of IκB kinase by vaccinia virus virulence factor B14. *PLoS Pathog.* **4,** e22 CrossRef Medline
45. Velázquez Campoy, A., and Freire, E. (2005) ITC in the post-genomic era? Priceless. *Biophys. Chem.* **115,** 115–124 CrossRef Medline
46. Walter, T. S., Meier, C., Assenberg, R., Au, K. F., Ren, J., Verma, A., Nettleship, J. E., Owens, R. J., Stuart, D. I., and Grimes, J. M. (2006) Lysine methylation as a routine rescue strategy for protein crystallization. *Structure* **14,** 1617–1622 CrossRef Medline
47. Tickle, I. J., Sharff, A., Flensburg, C., Smart, O., Keller, P., Vonrhein, C., Paciorek, W., and Bricogne, G. (2018) STARANISO. Global Phasing Ltd., Cambridge, United Kingdom
48. Clabbers, M. T. B., Gruene, T., Parkhurst, J. M., Abrahams, J. P., and Waterman, D. G. (2018) Electron diffraction data processing with DIALS. *Acta Crystallogr. D Struct. Biol.* **74,** 506–518 CrossRef Medline
49. Ahmad, K. F., Melnick, A., Lax, S., Bouchard, D., Liu, J., Kiang, C. L., Mayer, S., Takahashi, S., Licht, J. D., and Privé, G. G. (2003) Mechanism of SMRT corepressor recruitment by the BCL6 BTB domain. *Mol. Cell* **12,** 1551–1564 CrossRef Medline
50. Croll, T. I. (2018) ISOLDE: a physically realistic environment for model building into low-resolution electron-density maps. *Acta Crystallogr. D Struct. Biol.* **74,** 519–530 CrossRef Medline
51. Bricogne, G., Blanc, E., Brandl, M., Flensburg, C., Keller, P., Paciorek, W., Roversi, P., Sharff, A., Smart, O. S., Vonrhein, C., and Womack, T. O. (2017) BUSTER, Version 2.10.3. Global Phasing Ltd., Cambridge, United Kingdom
52. Mathew, R., Seiler, M. P., Scanlon, S. T., Mao, A. P., Constantinides, M. G., Bertozzi-Villa, C., Singer, J. D., and Bendelac, A. (2012) BTB-ZF factors recruit the E3 ligase cullin 3 to regulate lymphoid effector programs. *Nature* **491,** 618–621 CrossRef Medline
53. Zhang, D. D., Lo, S. C., Cross, J. V., Templeton, D. J., and Hannink, M. (2004) Keap1 is a redox-regulated substrate adaptor protein for a Cul3-dependent ubiquitin ligase complex. *Mol. Cell. Biol.* **24,** 10941–10953 CrossRef Medline
54. Liu, Z., Xiang, Y., and Sun, G. (2013) The KCTD family of proteins: structure, function, disease relevance. *Cell Biosci.* **3,** 45 CrossRef Medline
55. Neidel, S., Maluquer de Motes, C., Mansur, D. S., Strnadova, P., Smith, G. L., and Graham, S. C. (2015) Vaccinia virus protein A49 is an unexpected member of the B-cell lymphoma (Bcl)-2 protein family. *J. Biol. Chem.* **290,** 5991–6002 CrossRef Medline
56. Walter, T. S., Mancini, E. J., Kadlec, J., Graham, S. C., Assenberg, R., Ren, J., Sainsbury, S., Owens, R. J., Stuart, D. I., Grimes, J. M., and Harlos, K. (2008) Semi-automated microseeding of nanolitre crystallization experiments. *Acta Crystallogr. Sect. F Struct. Biol. Cryst. Commun.* **64,** 14–18 CrossRef Medline
57. Winter, G., Waterman, D. G., Parkhurst, J. M., Brewster, A. S., Gildea, R. J., Gerstel, M., Fuentes-Montero, L., Vollmar, M., Michels-Clark, T., Young, I. D., Sauter, N. K., and Evans, G. (2018) DIALS: implementation and evaluation of a new integration package. *Acta Crystallogr. D Struct. Biol.* **74,** 85–97 CrossRef Medline
58. Winter, G. (2010) xia2: an expert system for macromolecular crystallography data reduction. *J. Appl. Cryst.* **43,** 186–190 CrossRef
59. Evans, P. R., and Murshudov, G. N. (2013) How good are my data and what is the resolution? *Acta Crystallogr. D Biol. Crystallogr.* **69,** 1204–1214 CrossRef Medline
60. Bunkóczi, G., Echols, N., McCoy, A. J., Oeffner, R. D., Adams, P. D., and Read, R. J. (2013) Phaser.MRage: automated molecular replacement. *Acta Crystallogr. D Biol. Crystallogr.* **69,** 2276–2286 CrossRef Medline
61. Vagin, A., and Teplyakov, A. (2010) Molecular replacement with MOLREP. *Acta Crystallogr. D Biol. Crystallogr.* **66,** 22–25 CrossRef Medline
62. Winn, M. D., Ballard, C. C., Cowtan, K. D., Dodson, E. J., Emsley, P., Evans, P. R., Keegan, R. M., Krissinel, E. B., Leslie, A. G., McCoy, A., McNicholas, S. J., Murshudov, G. N., Pannu, N. S., Potterton, E. A., Powell, H. R., *et al.* (2011) Overview of the CCP4 suite and current developments. *Acta Crystallogr. D Biol. Crystallogr.* **67,** 235–242 CrossRef Medline
63. Emsley, P., Lohkamp, B., Scott, W. G., and Cowtan, K. (2010) Features and development of Coot. *Acta Crystallogr. D Biol. Crystallogr.* **66,** 486–501 CrossRef Medline
64. Murshudov, G. N., Vagin, A. A., and Dodson, E. J. (1997) Refinement of macromolecular structures by the maximum-likelihood method. *Acta Crystallogr. D Biol. Crystallogr.* **53,** 240–255 CrossRef Medline
65. Chen, V. B., Arendall, W. B., 3rd, Headd, J. J., Keedy, D. A., Immormino, R. M., Kapral, G. J., Murray, L. W., Richardson, J. S., and Richardson, D. C. (2010) MolProbity: all-atom structure validation for macromolecular crystallography. *Acta Crystallogr. D Biol. Crystallogr.* **66,** 12–21 CrossRef Medline
66. Sievers, F., and Higgins, D. G. (2018) Clustal Omega for making accurate alignments of many protein sequences. *Protein Sci.* **27,** 135–145 CrossRef Medline
67. Bond, C. S., and Schüttelkopf, A. W. (2009) ALINE: a WYSIWYG protein-sequence alignment editor for publication-quality alignments. *Acta Crystallogr. D Biol. Crystallogr.* **65,** 510–512 CrossRef Medline
68. Krissinel, E., and Henrick, K. (2007) Inference of macromolecular assemblies from crystalline state. *J. Mol. Biol.* **372,** 774–797 CrossRef Medline
69. Schrödinger, LLC (2015) *The PyMOL Molecular Graphics System,* Version 1.8., Schrödinger, LLC, New York
70. Eisenberg, D., Schwarz, E., Komaromy, M., and Wall, R. (1984) Analysis of membrane and surface protein sequences with the hydrophobic moment plot. *J. Mol. Biol.* **179,** 125–142 CrossRef Medline